Electronic K x rays emitted from muonic atoms: An application of relativistic density-functional theory

X. M. Tong [1,*] D. Kato [2,3] T. Okumura [4,5] S. Okada [4,6] and T. Azuma [4,†]

[1] *Center for Computational Sciences, University of Tsukuba, 1-1-1 Tennodai, Tsukuba, Ibaraki 305-8573, Japan*
[2] *National Institute for Fusion Science (NIFS), Toki, Gifu 509-5292, Japan*
[3] *Interdisciplinary Graduate School of Engineering Sciences, Kyushu University, Kasuga, Fukuoka 816-8580, Japan*
[4] *Atomic, Molecular and Optical Physics Laboratory, RIKEN, Wako 351-0198, Japan*
[5] *Department of Chemistry, Tokyo Metropolitan University, Hachioji, Tokyo 192-0397, Japan*
[6] *Center for Muon Science and Technology, Chubu University, Kasugai, Aichi 487-8501, Japan*

(Received 8 October 2022; accepted 21 December 2022; published 5 January 2023)

We develop a method using relativistic density-functional theory with a self-interaction correction, which is simple and fast yet has reasonable accuracy. A comparison with measured $K\alpha$ lines and their hypersatellites of several atoms, from low Z to high Z, reveals that the relativistic local density approximation is suitable for $K\alpha$ lines. In contrast, the relativistic local spin density approximation with a self-interaction correction is better for $K^h\alpha$ hypersatellites. Compared with the nonrelativistic density-functional theory, we found that the relativistic effect is significant (about 100 eV) even for middle-Z atoms, such as Cu. The screening effects, from inner shell to outer shell, and the conduction band, are also discussed. The present paper provides all the transition lines of muonic atoms, which can be used to narrow down the possible transitions by comparing them with the measurements.

DOI: 10.1103/PhysRevA.107.012804

I. INTRODUCTION

Muonic atoms, which have been studied extensively, are atoms with an electron replaced by a negatively charged muon [1]. A muon is about 200 times heavier than an electron, so it moves closer to the nucleus; muonic atoms thus connect atomic physics and nuclear physics [2–5]. When a muon is captured to a highly exited state by an atom, the muonic atom can emit two kinds of x rays. One is called a muonic x ray due to transitions between two muon states [6]. The other is called an electronic x ray due to transitions between two electron states [7,8]. X rays emitted from muonic atoms encode information of the muon state and the electron configuration of exotic atoms. Such information can be decoded by comparing the measured x-ray energies with the calculated ones. Muonic atoms have also been used to study the proton size [9], Lamb shift [10], and other higher-order effects [11,12], as well as a probe of local environments surrounding an exotic atom [13,14]. The transition energies can be calculated by various methods, from simple nonrelativistic Hartree-Fock-Slater methods [15], to more complex methods, such as the multiconfiguration Dirac-Fock and generalized matrix elements (MCDFGME) method [16,17], which includes quantum electrodynamics (QED), the Breit interaction, a finite nuclear size [5], and vacuum polarization [1,18]. Due to the recent development of low-energy muon beams [19] and new detector technologies [20], the electronic $K\alpha$ x rays emitted from muonic atoms can be measured to a high precision [21]. The most recently reported one was the measurement of electronic $K\alpha$ x rays from muonic Fe atomic ions [8]. These measured $K\alpha$ x rays are emitted from different muon states and ionic Fe states. The number of possible transitions is about a quarter million without considering the energy level splitting for the same electron configuration and different angular momentum couplings. If we consider all the atomic energy levels, the number could reach 10 million or more. We performed a simulation based on nonrelativistic density-functional theory (DFT) [22] and compared the results with experiment by shifting the energy systematically. These shifts are mainly attributed to relativistic effects.

Since similar experiments on other materials and atoms are being planned, it is necessary to develop a simple, fast method with reasonable accuracy to calculate all the transition energies. By comparing with the measured ones, one can narrow down the possible transitions, and then perform a more sophisticated simulation, such as the MCDFGME method. For such a goal, we extended the relativistic density-functional theory with a self-interaction correction for atoms [23] to exotic atoms. This method should, of course, also work for ordinary atoms. By comparing the measured $K\alpha$ and hypersatellite lines of atoms with the ones calculated by various exchange-correlation functionals, we found that the relativistic local density approximation (LDA) is more accurate for $K\alpha$ lines from low- to high-Z atoms, while for the $K^h\alpha$ hypersatellite, the relativistic local spin density approximation (LSDA) with self-interaction corrections (SIC) works better. Since our goal is to develop a simple, fast method, we used the simple LDA or LSDA exchange-correction functional [24,25], instead of

*tong.xiaomin.ga@u.tsukuba.ac.jp
†toshiyuki-azuma@riken.jp

using a more complicated exchange-correlation functional, such as the generalized gradient approximation (GGA) [26] or meta-GGA [27] with tunable parameters. The present method works for both muonic and electronic x rays.

Since our goal is to provide the electronic K x-ray energies for all charge states in order to identify possible transitions measured in the experiment, we do not present the muonic x-ray nor the transition rates. The transition rates can be calculated [28] once the transitions are identified or narrowed down.

We also studied the electron screening effects from different orbits and concluded that the outer screening (M shell, N shell, and the conduction band in the solid) is not important. This justifies our use of the isolated muonic Fe data to compare with the measurements from an Fe foil.

II. THEORETICAL METHOD

The descriptions of density-functional theory with a self-interaction correction for atoms can be found in Refs. [22,23]. Here, we only present the working equations for exotic atoms. In the relativistic density-functional theory, the Dirac equation of the electrons in an exotic atom is written as (atomic units $\hbar = m_e = e = 1$ are used unless stated otherwise)

$$[c\boldsymbol{\alpha} \cdot \boldsymbol{p} + \beta c^2 + v_{\mathrm{eff},\sigma}(\mathbf{r})]\psi_{i\sigma}(\mathbf{r}) = \epsilon_{i\sigma}\psi(\mathbf{r}). \qquad (1)$$

The Dirac equation of the muon in the exotic atom is written as

$$[c\boldsymbol{\alpha} \cdot \boldsymbol{p}_\mu + m_\mu \beta c^2 + v_\mu(\mathbf{r}_\mu)]\psi_\mu(\mathbf{r}_\mu) = \epsilon_\mu \psi_\mu(\mathbf{r}_\mu). \qquad (2)$$

Here, m_μ is the muon mass, c is the light velocity in vacuum, and $\mathbf{r}$, $\mathbf{r}_\mu$ are the electron and muon coordinates, respectively. The electron moves in an optimized effective potential [29], plus the electron-muon interaction as

$$v_{\mathrm{eff},\sigma}(\mathbf{r}) = V^{\mathrm{OEP}}(\mathbf{r}) + \int \frac{\rho_\mu(\mathbf{r}_\mu)}{|\mathbf{r} - \mathbf{r}_\mu|} d\mathbf{r}_\mu, \qquad (3)$$

and the muon moves in an effective potential formed by the nucleus and the electrons as

$$v_\mu(\mathbf{r}_\mu) = V_N(\mathbf{r}_\mu) + \int \frac{\rho_e(\mathbf{r})}{|\mathbf{r} - \mathbf{r}_\mu|} d\mathbf{r}. \qquad (4)$$

Here, V^{OEP} is the optimized effective potential [29,30], which can be obtained as detailed in Refs. [23,31] and the last term in Eq. (3) represents the muon-electron interaction. V_N is the muon-nucleus interaction, and the last term in Eq. (4) is the electron-muon interaction. ρ_e, ρ_μ are the electron and muon charge densities, respectively. Equations (1)–(4) are solved iteratively (self-consistently) until the effective potentials reach convergence. The total energy for a given electron configuration and muon state is obtained, and the emitted x-ray energy is calculated as the total energy difference between the transition initial and final states.

We used the pseudospectra grid [32,33] to discretize the space for the electron and muon radial wave functions separately due to the mass difference between the muon and electron. If we replace the Dirac equations with Schrödinger equations, we get the nonrelativistic version [22] of the DFT method for exotic atoms.

III. RESULTS AND DISCUSSION

Within the DFT method, there are many exchange-correlation functionals (several tens or hundreds), from LSDA (LDA) to meta-GGA [34]. Even for the simplest LDA, one can still consider the self-interaction correction (SIC). Our goal is to find a simple, fast, yet reliable method to estimate electronic K x-ray energies and their hypersatellite energies for muonic atoms. By setting the muon density to zero, the method should also work for characteristic K x rays emitted from an atom with one $1s$ vacancy, which has been studied extensively [35]; these data, from both theory and experiment, are tabulated in Ref. [36]. Data also exist [37,38] for K x-ray hypersatellites emitted from hollow atoms with two $1s$ vacancies. Therefore, we first compare the characteristic x-ray energies calculated by DFT methods with LSDA or LDA with or without SIC to find which exchange-correlation functional is better for K x rays of atoms. Here, we labeled the relativistic DFT with a local spin density approximation with a self-interaction correction as R-LSDA/SIC and without SIC as R-LSDA/non-SIC and DFT with a local density approximation with SIC as R-LDA/SIC and without SIC as R-LDA/non-SIC. To study the relativistic effects, we also present the corresponding non-relativistic ones labeled as NR-LSDA or NR-LDA. First, we compare our results with other existing data for the case of ordinary atoms to check the validity of the present method.

A. K x ray and its hypersatellite of atoms

Table I lists the reported $K\alpha_{1,2}, K\beta_1$ energies for the low-Z atom Ar ($Z = 18$), the high-Z atom Rn ($Z = 86$), and the spin-polarized atom Eu ($Z = 63$), and the energy differences between experiments and calculations with the relativistic and nonrelativistic DFT methods using various exchange-correlation functionals. The hypersatellites $K^h\alpha_{1,2}$ from Cu [38] and Pb atoms [37] are also listed. For the theoretical results, we only present the energy difference with the measured one, which is defined as $\Delta = E_{\mathrm{expt}} - E_{\mathrm{theor}}$. Overall, the results of the relativistic simulations are better than the nonrelativistic ones: The maximum error for the relativistic simulation is less than 0.5%, while the nonrelativistic results are in reasonable agreement with the measured ones only for low-Z atoms, such as Ar, as we expected. For high-Z atoms, such as Rn, the relativistic effect is about 10%. Note that for the nonrelativistic simulation, we cannot distinguish $K\alpha_1$ and $K\alpha_2$. Therefore, a relativistic calculation is needed even for a low-Z atom, such as Ar. For high-Z atoms, the relativistic effects cannot be ignored. For the nonrelativistic simulation, the results are not so sensitive to SIC or non-SIC for high-Z atoms because the relativistic effect is the major error source. For low-Z atoms, the results of LSDA/SIC are better for ionization potentials, as reported in a previous work [23]. Indeed, the NR-LDA/SIC results for Ar atoms are the best among the nonrelativistic simulations. Thus, we may think that the results of the relativistic SIC should also be better than the non-SIC ones. To our surprise, the K x-ray energies calculated with R-LDA without SIC are better than the ones with SIC. For all of the K x rays in the table, the maximum relative error of R-LDA/non-SIC is less than 0.05%. For a very heavy atom, such as Rn, the R-LDA/non-SIC and R-LSDA/

TABLE I. Transition energies of $K\alpha_{1,2}$, $K\beta_1$ for Ar, Rn, and Eu atoms and $K^h\alpha_{1,2}$ hypersatellites for Cu and Pd atoms from experiments. The energy differences between the experiments and the simulations are also presented. All the energies are in eV. The bold font highlights the best performing method for a given case.

			R-LSDA		R-LDA		NR-LSDA		NR-LDA	
Element		E_{expt}	SIC	Non-SIC	SIC	Non-SIC	SIC	Non-SIC	SIC	Non-SIC
Ar[a] ($Z = 18$)	$K\alpha_1$	2957.68	2.29	17.80	−15.85	**−0.26**	14.33	28.09	−4.05	9.76
	$K\alpha_2$	2955.57	2.55	18.04	−15.58	**0.02**	12.22	25.98	−6.16	7.65
	$K\beta_1$	3190.49	0.62	18.84	−18.53	**−0.22**	11.94	28.41	−7.45	9.08
Rn[a] ($Z = 86$)	$K\alpha_1$	83783	−315	11	−363	**−36**	10508	10580	10430	10502
	$K\alpha_2$	81066	−282	37	−328	**−10**	7791	7863	7713	7785
	$K\beta_1$	94867	−319	31	−371	**−21**	10503	10595	10420	10512
Eu[a] ($Z = 63$)	$K\alpha_1$	41542.63	−96.17	45.43	−142.67	**−0.77**	2588.43	2640.53	2530.23	2582.33
	$K\alpha_2$	40902.33	−83.57	55.73	−129.67	**10.03**	1948.13	2000.23	1889.93	1942.03
	$K\beta_1$	47038.40	−103.60	53.30	−151.60	**5.50**	2568.30	2634.50	2504.80	2571.10
Cu[b] ($Z = 29$)	$K^h\alpha_1$	8352.60	**−2.35**	29.87	26.28	58.39	107.82	131.62	137.48	161.22
	$K^h\alpha_2$	8329.10	**−1.85**	30.31	26.57	58.51	84.32	108.12	113.98	137.72
Pb[c] ($Z = 82$)	$K^h\alpha_1$	76250±60	**−133**	157	80	210	8876	8945	8953	9022

[a]Reference [36]
[b]Reference [38]
[c]Reference [37]

non-SIC results are comparable. A possible reason is that there are two 1s electrons in the transition final state, thereby, the spin average is better than the self-interaction correction, or there are some cancellations between the relativistic effect and the self-interaction correction. The original motivation for introducing SIC [39] is to correct for the long-range Coulomb tail, which significantly improves the orbital energies [22] while only moderately improving the total energies [31]. We use the total energy difference to calculate the transition energies, not the orbital energies. Also, the SIC corresponds to a single-electron correction, and its relative contribution is smaller for many-electron atoms or high-Z atoms. This could be another possible reason why R-LDA/non-SIC is better for the K x rays. For a given transition, the number of 1s electrons in the final state plays an important role.

To check this scenario, we studied the K x-ray hypersatellites (the final state having only one 1s electron) where the local spin density approximation with a self-interaction correction plays a crucial role. In the R-LSDA/SIC, we assume that the electron spin flip is forbidden and the transition happens only among the same spin states. Indeed, we found that the R-LSDA/SIC is better for the K x-ray hypersatellites of Cu. For heavy atoms, such as Pb ($Z = 82$), both R-LSDA/SIC and R-LDA/SIC are better than the others. For such a heavy atom, the Breit interaction [40], which is about several tens of eV [41,42], is ignored in the present simulation.

To confirm the reliability of the R-LSDA/SIC, Table II lists the $K^h\alpha$ hypersatellite energies of the 3d transition metals reported in Ref. [38] and the values of the relativistic multiconfiguration Dirac-Fock (RMCDF) methods [41,44,45] and the active space approximation (ASA) methods [43]. To focus on the reliability of the simulations, we present the experimental results along with the differences between the measured ones and simulations as $\Delta = E_{\mathrm{expt}} - E_{\mathrm{theor}}$.

For $K^h\alpha_2$ x rays, our results are comparable with other simulations, and the errors are less than 5 eV for all elements in Table II. For $K^h\alpha_1$ x rays, the results of Ref. [43] are better than ours, but the largest error of our results is still less than 10 eV. Overall, our results are comparable with RMCDF-type simulations, but numerically much simpler and faster. The present DFT method is equivalent to the level average of RMCDF without calculating all of the energy levels for the same electron configuration and different total angular momenta. We need to calculate three total energies for the $K^h\alpha_1$, $K^h\alpha_2$ transition energies: One initial and two final states. It took less than a minute with a desktop computer. The present method is highly parallelized for use with a many-core computer or even a supercomputer. Thus we can estimate the K x-ray energy quickly.

Note that the above numerical results depend weakly on the simulation parameters, such as the box size and the number of grids. The results may change within a few eV for heavy atoms if we reduced the box size and the number of grids by half. In the present simulation, we did not tune these parameters and used a box size of $R_{\max} = 20$ a.u. with the number of grids $N = 320$. We found that the R-LDA/non-SIC is better

TABLE II. $K^h\alpha_{1,2}$ hypersatellite energies of the 3d transition metals reported in Ref. [38]. The energy differences between the experiment and present simulations (Δ_p) with R-LDA/SIC and the differences between the experiment and the results of RMCDF (Δ_{R}) [38] or ASA (Δ_{A}) [43] methods are also presented. All energies are in eV.

Element	$K^h\alpha_2$	Δ_p	Δ_{R}	Δ_{A}	$K^h\alpha_1$	Δ_p	Δ_{A}
V	5176.6	0.89	1.50		5191.7	7.27	
Cr	5649.2	0.56	0.70	0.8	5665.1	5.96	0.9
Mn	6143.4	1.00	2.80		6160.9	5.92	
Fe	6659.7	2.53	4.00	2.7	6678.8	6.69	2.9
Co	7194.4	1.10	3.10		7214.9	4.00	
Ni	7752.3	1.43	3.00		7774.1	2.62	
Cu	8329.1	−1.85	−0.20		8352.6	−2.35	
Zn	8929.5	−1.17	0.60	0.6	8955.8	−2.65	0.4

TABLE III. Energy shifts (in eV) of $K\alpha$ lines of μFe from the $K\alpha$ of Mn atoms calculated with R-LDA/non-SIC.

μ-state	Present	NR-LDA[a]	NR-HF [15]	RMCDF
1*s*	0.0	0.0	0.0	−0.6
5*s*	13.4	12.5	11.9	12.6
10*s*	119.8	114.9	112.9	118.3

[a]Note that the results are slightly different from the values in the Supplemental Material of Ref. [8] due to the values being calculated with NR-LSDA/SIC.

for K x rays and R-LSDA/SIC works better for K^h hypersatellites. Therefore, in the following discussion, all the results are obtained with the R-LDA/non-SIC for muonic atoms or ions since only the electronic $K\alpha$ transitions of muonic Fe were reported in a recent experiment [8]. Of course, our method should also work for $K^h\alpha$ hypersatellites.

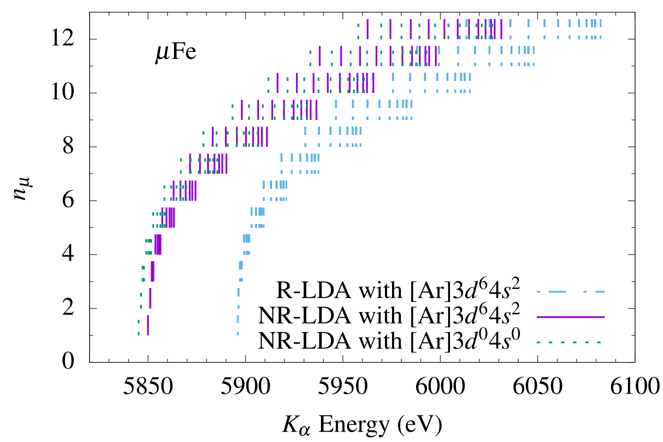

FIG. 1. $K\alpha$ energies of μFe as a function of muonic states (n_μ, l_μ, or j_μ) calculated by the LDA/non-SIC methods. For the relativistic simulation, only $K\alpha_1$ lines are presented.

B. Energy shifts of electronic K x ray of muonic Fe

The muon is initially captured in highly excited states peaked at a principal quantum number of about $n \approx \sqrt{m_\mu} \approx 14$ for low incident energies close to the threshold; the peak moves to higher n as the incident energy increases [46,47]. Then the muon gradually cascades into lower excited states through Auger decay by removing electrons from Fe atomic ions or through radiative decay by losing energy via emitting a photon. The cascade process has been studied in Refs. [48,49]. During the cascading, various charged hollow ions are formed. We first analyze the transition energy shifts of K x rays with different muon states for muonic Fe (μFe) with only one K vacancy. There are no high-precision experimental data for muon state-specified electronic K x rays. Thus we use the MCDFGME [8] data as references. The energy shifts are almost the same for $K\alpha_{1,2}$, and we do not distinguish the two lines. Table III lists the $K\alpha$ energy shifts of muonic Fe atoms with respect to the $K\alpha$ line of Mn atoms. As the muon state n_μ becomes lower, the screening effect of the muon on the nucleus becomes more significant, and at $n_\mu = 1$, $K\alpha$ lines of μFe become identical to $K\alpha$ of Mn atoms. Overall, our results are in reasonable agreement with the nonrelativistic Hartree-Fock results [15], although the $K\alpha$ energies may differ due to relativistic effects. Our results are also in agreement with MCDFGME [8], in which QED and other higher-order effects are considered. The discrepancies between the present simulations and MCDFGME ones are less than 2 eV.

C. Electronic $K\alpha$ x rays from muonic Fe ions

There are various types of μFe ions with different charge states formed during the cascade process. In the solid state, the vacancies of the hollow ions can be refilled by electrons in the conduction band. We need to consider all muon states from $n = 1$ to $n = 12$, which is 144 states if all possible j states are considered. The probability for a muon captured into a high-n (>12) state with a K vacancy is negligibly small. For spin-averaged simulations with LDA, the number of electron configurations of the L shell with the electron number varying from 0 to 8 is 45, which is the same for the M shell. Therefore, the total transition lines are $144 \times 45 \times 45 = 291\,600$, roughly a quarter million. If we consider all energy levels with the same electron configuration and different total angular momenta, the number can easily reach for 10 million or even more. This is our motivation for a simple, fast method to estimate $K\alpha$ energies of muonic atoms and ions.

Since the experiment was performed with an Fe foil, we need to check if the conduction band electrons affect the x-ray energies emitted from hollow muonic Fe ions produced in the metal. We modified the method employed to study x-ray emission from hollow nitrogen ions N^{q+} inside of a metal in Ref. [50] to study muonic atomic ions in a metal. For N^{q+} ions in Al metal, the emitted x-ray energies differ from the corresponding emission in vacuum. The energy shifts also depend on the charge state q. Unlike N^{q+} hollow atoms, x-ray energies from μFe hollow ions in bulk are almost the same as the ones in vacuum. By further analysis, we confirmed that the screening effect of electrons in the conduction band on μFe is attributed to an outer screening that does not affect the $K\alpha$ transition energies. This is different from the case of N^{q+} hollow atoms in bulk, in which the screening affects the initial state of the transition. Therefore, all of the following μFe results are calculated for isolated μFe atomic ions.

Figure 1 shows the electronic $K\alpha$ (or $K\alpha_1$ for the relativistic case) energies of μFe ions with different muon states determined by the relativistic and nonrelativistic LDA simulations. To show the outer screening effect, we plot the data of μFe ions where all the valence electrons in 3d, 4s orbits are removed for the nonrelativistic LDA simulation. For a given principal quantum number n_μ, there are still many possible j_μ or l_μ states, which results in a spreading of the energy. Note that the outer screening effect becomes negligibly small by removing the eight valence electrons. This screening effect should be larger than the screening from the electrons in the conduction band. This comparison justifies using μFe data to compare with the ones measured in a solid [8]. We also see that the relativistic effect shifts the nonrelativistic results systematically, and the shifts weakly depend on the muon states. The nonrelativistic shift of this calculation is 47 eV, and the value of MCDFGME is 50 eV [51]. This justifies the

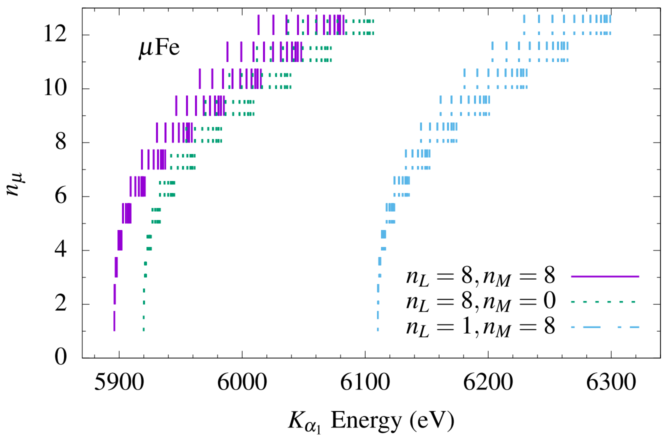

FIG. 2. $K\alpha_1$ energies of μFe as a function of muonic states (n_μ, j_μ) with different numbers of M, L-shell electrons calculated by the relativistic LDA method.

procedure in Ref. [8], where we used the nonrelativistic results and shifted by a constant value systematically.

Figure 2 shows $K\alpha_1$ energies of μFe ions with different muon states determined by the relativistic LDA simulations for changing the number of electrons in the M and L shells. Comparing $K\alpha_1$ with a full $3s^2 3p^6$ and without $3s, 3p$ electrons, the screening effect of the $3s, 3p$ can be as large as 20 eV. This is not negligibly small, and the electron configuration in the M shell should be taken into account for a high-precision simulation. Comparing the results with the full L-shell electrons and one L-shell electron, we found the energy shifts can be as large as 200 eV. This shows that the L-shell electron is important for the $K\alpha$ transition, and the electron configuration in the L shell must be considered. The different muon states also contribute to the $K\alpha$ energy, and the measured x-ray energy encodes the information of the muon states and the electron configurations of μFe ions.

As we mentioned that there are about a quarter million $K\alpha$ lines in the simulation, we do not present all of them but use the data to compare with the measurements.

IV. CONCLUSION

We developed a relativistic density-functional theory to study electronic $K\alpha$ x-ray energies of muonic atoms. By comparing the available $K\alpha$ and its hypersatellite energies calculated with various exchange-correlation functionals for various atoms, from low- to high-Z atoms, we conclude that (1) while relativistic effects are obviously important for high-Z atoms, which are known qualitatively without simulation, even for middle-Z atoms relativistic simulations are necessary; (2) the relativistic local density approximation is suitable for $K\alpha$ while the relativistic local spin density approximation with a self-interaction correction is suitable for hypersatellites. We also studied the screening effect from electrons in the inner-shell/outer-shell orbits and the conduction band. We found that the outer screening effect from the conduction band and valence electrons is negligibly small (about a few eV for muonic Fe ions). In contrast, the inner-shell (L-shell) screening effect is comparable to or even larger than the energy shifts from different muon states. Such a simple, fast, reasonably accurate method can be used to calculate all K x-ray energies, either muonic x rays or electronic x rays. The number of the transitions can reach about a quarter million, even a million depending on the targets. Comparing the simulations by this method with experiments, one can narrow down the possible transitions and then study the specific transitions with a more elaborate method, such as MCDFGME with QED and other higher-order effects.

All data are available from the corresponding author (X.M.T.) upon request.

ACKNOWLEDGMENTS

This work was supported by the Multidisciplinary Cooperative Research Program in Center for Computational Sciences, University of Tsukuba. X.M.T. was supported by the JSPS KAKENHI (Grant-in-Aid for Scientific Research (C) 22K03493. T.A., T.O., and S.O. were supported by the JSPS KAKENHI (Grant-in-Aid for Scientific Research on Innovative Areas, Toward new frontiers: Encounter and synergy of state-of-the-art astronomical detectors and exotic quantum beams 18H05457 and 18H05458, Grant-in-Aid for Scientific Research (A) 18H03714, and Grant-in-Aid for Young Scientists 20K15238), and the RIKEN Pioneering Projects. We are grateful to Professor P. Indelicato for providing MCDFGME data.

[1] E. Borie and G. A. Rinker, The energy levels of muonic atoms, Rev. Mod. Phys. **54**, 67 (1982).

[2] D. Measday, The nuclear physics of muon capture, Phys. Rep. **354**, 243 (2001).

[3] T. Gorringe and D. Hertzog, Precision muon physics, Prog. Part. Nucl. Phys. **84**, 73 (2015).

[4] A. Knecht, A. Skawran, and S. M. Vogiatzi, Study of nuclear properties with muonic atoms, Eur. Phys. J. Plus **135**, 777 (2020).

[5] I. A. Valuev, G. Colò, X. Roca-Maza, C. H. Keitel, and N. S. Oreshkina, Evidence Against Nuclear Polarization as Source of Fine-Structure Anomalies in Muonic Atoms, Phys. Rev. Lett. **128**, 203001 (2022).

[6] F. J. Hartmann, T. von Egidy, R. Bergmann, M. Kleber, H. J. Pfeiffer, K. Springer, and H. Daniel, Measurement of the Muonic X-Ray Cascade in Metallic Iron, Phys. Rev. Lett. **37**, 331 (1976).

[7] H. Schneuwly and P. Vogel, Electronic K x-ray energies in heavy muonic atoms, Phys. Rev. A **22**, 2081 (1980).

[8] T. Okumura, T. Azuma, D. A. Bennett, P. Caradonna, I. Chiu, W. B. Doriese, M. S. Durkin, J. W. Fowler, J. D. Gard, T. Hashimoto, R. Hayakawa, G. C. Hilton, Y. Ichinohe, P. Indelicato, T. Isobe, S. Kanda, D. Kato, M. Katsuragawa, N. Kawamura, Y. Kino *et al.*, Deexcitation Dynamics of Muonic Atoms Revealed by High-Precision Spectroscopy of Electronic K X Rays, Phys. Rev. Lett. **127**, 053001 (2021).

[9] R. Pohl, R. Gilman, G. A. Miller, and K. Pachucki, Muonic hydrogen and the proton radius puzzle, Annu. Rev. Nucl. Part. Sci. **63**, 175 (2013).

[10] C. Ji, N. Nevo Dinur, S. Bacca, and N. Barnea, Nuclear Polarization Corrections to the $\mu^4\mathrm{He}^+$ Lamb Shift, Phys. Rev. Lett. **111**, 143402 (2013).

[11] I. Beltrami, B. Aas, W. Beer, G. D. Chambrier, P. Goudsmit, T. Ledebur, H. Leisi, W. Ruckstuhl, W. Sapp, G. Strassner, A. Vacchi, U. Kiebele, J.-A. Pinston, and R. Weber, New precision measurements of the muonic x-ray transition in ^{24}Mg and ^{28}Si: Vacuum polarisation test and search for muon-hadron interactions beyond QED, Nucl. Phys. A **451**, 679 (1986).

[12] N. Michel and N. S. Oreshkina, Higher-order corrections to the dynamic hyperfine structure of muonic atoms, Phys. Rev. A **99**, 042501 (2019).

[13] T. Siems, D. F. Anagnostopoulos, G. Borchert, D. Gotta, P. Hauser, K. Kirch, L. M. Simons, P. El-Khoury, P. Indelicato, M. Augsburger, D. Chatellard, and J.-P. Egger, First Direct Observation of Coulomb Explosion during the Formation of Exotic Atoms, Phys. Rev. Lett. **84**, 4573 (2000).

[14] M. Aramini, C. Milanese, A. D. Hillier, A. Girella, C. Horstmann, T. Klassen, K. Ishida, M. Dornheim, and C. Pistidda, Using the emission of muonic x-rays as a spectroscopic tool for the investigation of the local chemistry of elements, Nanomaterials **10**, 1260 (2020).

[15] T. Mukoyama, Electronic K-x-ray transitions in light muonic atoms, Eur. Phys. J. D **73**, 75 (2019).

[16] J. Desclaux, A multiconfiguration relativistic DIRAC-FOCK program, Comput. Phys. Commun. **9**, 31 (1975).

[17] P. Indelicato, E. Lindroth, and J. P. Desclaux, Nonrelativistic Limit of Dirac-Fock Codes: The Role of Brillouin Configurations, Phys. Rev. Lett. **94**, 013002 (2005).

[18] M. S. Dixit, A. L. Carter, E. P. Hincks, D. Kessler, J. S. Wadden, C. K. Hargrove, R. J. McKee, H. Mes, and H. L. Anderson, New Muonic-Atom Test of Vacuum Polarization, Phys. Rev. Lett. **35**, 1633 (1975).

[19] W. Higemoto, R. Kadono, N. Kawamura, A. Koda, K. Kojima, S. Makimura, S. Matoba, Y. Miyake, K. Shimomura, and P. Strasser, Materials and life science experimental facility at the Japan Proton Accelerator Research Complex IV: The muon facility, Quantum Beam Sci. **1**, 11 (2017).

[20] J. N. Ullom and D. A. Bennett, Review of superconducting transition-edge sensors for x-ray and gamma-ray spectroscopy, Supercond. Sci. Technol. **28**, 084003 (2015).

[21] S. Okada, T. Azuma, D. A. Bennett, P. Caradonna, W. B. Doriese, M. S. Durkin, J. W. Fowler, J. D. Gard, T. Hashimoto, R. Hayakawa, G. C. Hilton, Y. Ichinohe, P. Indelicato, T. Isobe, S. Kanda, M. Katsuragawa, N. Kawamura, Y. Kino, Y. Miyake, K. M. Morgan *et al.*, X-ray spectroscopy of muonic atoms isolated in vacuum with transition edge sensors, J. Low Temp. Phys. **200**, 445 (2020).

[22] X.-M. Tong and S.-I Chu, Density-functional theory with optimized effective potential and self-interaction correction for ground states and autoionizing resonances, Phys. Rev. A **55**, 3406 (1997).

[23] X.-M. Tong and S.-I Chu, Relativistic density-functional theory with the optimized effective potential and self-interaction correction: Application to atomic structure calculations ($Z =$ 2–106), Phys. Rev. A **57**, 855 (1998).

[24] P. A. M. Dirac, Note on exchange phenomena in the Thomas atom, Math. Proc. Cambridge Philos. Soc. **26**, 376 (1930).

[25] S. H. Vosko, L. Wilk, and M. Nusair, Accurate spin-dependent electron liquid correlation energies for local spin density calculations: A critical analysis, Can. J. Phys. **58**, 1200 (1980).

[26] J. P. Perdew, J. A. Chevary, S. H. Vosko, K. A. Jackson, M. R. Pederson, D. J. Singh, and C. Fiolhais, Atoms, molecules, solids, and surfaces: Applications of the generalized gradient approximation for exchange and correlation, Phys. Rev. B **46**, 6671 (1992).

[27] J. Tao, J. P. Perdew, V. N. Staroverov, and G. E. Scuseria, Climbing the Density Functional Ladder: Nonempirical Meta–Generalized Gradient Approximation Designed for Molecules and Solids, Phys. Rev. Lett. **91**, 146401 (2003).

[28] M. H. Chen, B. Crasemann, K. R. Karim, and H. Mark, Relativistic Auger and x-ray deexcitation rates of highly stripped atoms, Phys. Rev. A **24**, 1845 (1981).

[29] J. D. Talman and W. F. Shadwick, Optimized effective atomic central potential, Phys. Rev. A **14**, 36 (1976).

[30] R. T. Sharp and G. K. Horton, A variational approach to the unipotential many-electron problem, Phys. Rev. **90**, 317 (1953).

[31] Y. Li, J. B. Krieger, and G. J. Iafrate, Self-consistent calculations of atomic properties using self-interaction-free exchange-only Kohn-Sham potentials, Phys. Rev. A **47**, 165 (1993).

[32] J. Wang, S.-I Chu, and C. Laughlin, Multiphoton detachment of H^-. II. Intensity-dependent photodetachment rates and threshold behavior—complex-scaling generalized pseudospectral method, Phys. Rev. A **50**, 3208 (1994).

[33] D. A. Telnov and S.-I Chu, Multiphoton detachment of H^- near the one-photon threshold: Exterior complex-scaling-generalized pseudospectral method for complex quasienergy resonances, Phys. Rev. A **59**, 2864 (1999).

[34] M. A. Marques, M. J. Oliveira, and T. Burnus, Libxc: A library of exchange and correlation functionals for density functional theory, Comput. Phys. Commun. **183**, 2272 (2012).

[35] R. D. Deslattes, E. G. Kessler, P. Indelicato, L. de Billy, E. Lindroth, and J. Anton, X-ray transition energies: New approach to a comprehensive evaluation, Rev. Mod. Phys. **75**, 35 (2003).

[36] R. Deslattes, E. G. Kessler, Jr., P. Indelicato, L. de Billy, E. Lindroth, J. Anton, J. Coursey, D. Schwab, J. Chang, R. Sukumar, K. Olsen, and R. Dragoset, X-ray transition energies database, NIST Standard Reference Database 128, doi:10.18434/T4859Z (2005).

[37] J. Briand, P. Chevalier, A. Johnson, J. Rozet, M. Tavernier, and A. Touati, Experimental determination of the energy of K hypersatellite lines for various elements, Phys. Lett. A **49**, 51 (1974).

[38] R. Diamant, S. Huotari, K. Hämäläinen, R. Sharon, C. C. Kao, and M. Deutsch, $K^h\alpha_{1,2}$ hypersatellites of $3d$ transition metals and their photoexcitation energy dependence, Phys. Rev. A **79**, 062511 (2009).

[39] J. P. Perdew and A. Zunger, Self-interaction correction to density-functional approximations for many-electron systems, Phys. Rev. B **23**, 5048 (1981).

[40] G. Breit, The fine structure of He as a test of the spin interactions of two electrons, Phys. Rev. **36**, 383 (1930).

[41] A. M. Costa, M. C. Martins, J. P. Santos, P. Indelicato, and F. Parente, Relativistic calculation of $K\alpha$ hypersatellite line energies and transition probabilities for selected atoms

with $12 \leqslant Z \leqslant 80$, J. Phys. B: At., Mol. Opt. Phys. **40**, 57 (2007).
[42] X. M. Tong, N. Nakamura, S. Ohtani, T. Watanabe, and N. Toshima, Green's function for multielectron ions and its application to radiative recombination involving dielectronic recombinations, Phys. Rev. A **80**, 042502 (2009).
[43] L. Natarajan, Relativistic fluorescence yields for hollow atoms in the range $12 \leqslant Z \leqslant 56$, Phys. Rev. A **78**, 052505 (2008).
[44] M. C. Martins, A. M. Costa, J. P. Santos, F. Parente, and P. Indelicato, Relativistic calculation of two-electron one-photon and hypersatellite transition energies for $12 \leqslant Z \leqslant 30$ elements, J. Phys. B: At., Mol. Opt. Phys. **37**, 3785 (2004).
[45] P. Jönsson, X. He, C. F. Fischer, and I. P. G. and, The grasp2k relativistic atomic structure package, Comput. Phys. Commun. **177**, 597 (2007).
[46] J. S. Cohen, Isotope effects on antiproton and muon capture by hydrogen and deuterium atoms and molecules, Phys. Rev. A **59**, 1160 (1999).
[47] X. M. Tong, T. Shirahama, K. Hino, and N. Toshima, Time-dependent approach to three-body rearrangement collisions: Application to the capture of heavy negatively charged particles by hydrogen atoms, Phys. Rev. A **75**, 052711 (2007).
[48] V. Akylas and P. Vogel, Muonic atom cascade program, Comput. Phys. Commun. **15**, 291 (1978).
[49] P. Vogel, Muonic cascade: General discussion and application to the third-row elements, Phys. Rev. A **22**, 1600 (1980).
[50] X. M. Tong, D. Kato, T. Watanabe, H. Shimizu, C. Yamada, and S. Ohtani, Energy structure of hollow atoms or ions in the bulk of metallic materials, Phys. Rev. A **63**, 052505 (2001).
[51] P. Indelicato (private communication).